Study on Sloshing Flows and Flexible Baffle Motion inside a Rectangular Tank under Forced Harmonic Excitation

Taehyun Park[1], Yonghwan Kim[1], Cheon-Jin Park[2]
[1] Department of Naval Architecture and Ocean Engineering, Seoul National University, Republic of Korea
[2] Hyundai Maritime Research Institute, HD Hyundai Heavy Industries, Republic of Korea
thth0325@snu.ac.kr

1 INTRODUCTION

Sloshing in a partially-filled liquid tank is governed by fluid properties, filling height, and externally imposed tank motion. Since most sloshing flows in marine engineering are highly nonlinear, there are some critical technical barriers in accurate prediction. If there are internal structures, those can modify the flow field and alter the resonance characteristics. Sloshing in tanks with internal structures has been widely studied using potential theory and/or numerical methods. Focusing on the eigenvalues of sloshing flow with internal structure, we can find some pioneering works by Evans & MacIver (1987), Jeyakumaran & McIver (1994) for rigid internal baffle, and various problems can be found in the book of Faltinsen & Timokha (2009). More recently, sloshing with flexible internal structures was tackled by Meng et al. (2021), Ren et al. (2023), and Park et al. (2025).

The present study investigates sloshing in a rectangular tank with a vertical beam-type baffle mounted at the bottom center, considering both rigid and flexible configurations. An eigenvalue analysis is employed to characterize the coupled modal properties, and the results are compared with model-scale experiments and numerical simulations to clarify the role of structural flexibility in sloshing resonance and provide reference data for validating hydroelastic sloshing models.

2 EIGENVALUE ANALYSIS FOR SLOSHING NATURAL MODES

The eigenvalue problem of sloshing in a 2D rectangular tank with a vertical baffle (Fig.1) can be formulated to the following boundary value problem:

$$\phi(x,\mathrm{y},t)=\mathbb{R}\left\{\Phi(x,y)e^{i\omega t}\right\} \tag{1}$$

$$\nabla^2\Phi=0 \quad \text{in } \Omega \tag{2}$$

$$\frac{\partial\Phi}{\partial y}+K\Phi=0 \quad \text{on } S_F, \qquad K=\frac{\omega^2}{g} \tag{3}$$

$$\nabla\Phi\bullet\vec{n}=0 \quad \text{on } S_W,\ S_B \tag{4}$$

$$\frac{\partial\Phi}{\partial x}=\begin{cases}0 & \text{for rigid baffle}\\ i\omega\sum A_nW_n(y) & \text{for flexible baffle}\end{cases} \quad \text{on } S_C \tag{5}$$

where $W_n(y)$ and A_n are modal deflection and its amplitude.

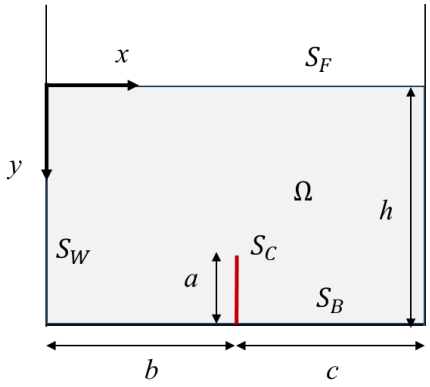

Figure 1: Schematic diagram and notation for a 2D rectangular tank

In the case of rigid baffle, following the approach of Evans & McIver (1987), the problem is reformulated in terms of the horizontal gap velocity, and an exact eigenvalue condition that may be expressed in the determinant form

$$\det\left(\mathbf{C}-A(K)\mathbf{B}\right)=0\,. \tag{6}$$

Here, **C** denotes the uncoupled sloshing operator of the non-compartmented tank, **B** represents the modal coupling induced by the baffle, and $A(K)$ is a coupling scalar coefficient depending on the eigenvalue K.

Considering the uncoupled sloshing modes of the tank without the internal baffle, *m* denotes the sloshing mode index, and the wavenumber and eigenvalue are expressed by $k_m (= m\pi/(b+c))$ and $K_m (= \tanh(k_m h))$, respectively.

Linearizing the determinant condition about wavenumber $k = k_m$ yields

$$k \approx k_m + \Delta k, \quad \Delta k \approx \frac{(-1)^m}{d} \frac{\sin(k_m b)\sin(k_m c)}{A}. \tag{7}$$

Accordingly, the sloshing eigenvalue can be approximated as

$$K \approx K_m + \left[\tanh(k_m h) + k_m h \operatorname{sech}^2(k_m h)\right] \Delta k. \tag{8}$$

If the internal baffle is thin and can be considered as a small structure, Jeyakumaran & McIver (1994) derived analytic formula for a few representative cases, and the eigenvalue for a single bottom-mounted baffle can be written as

$$K = K_M - \frac{\pi a^2 k_M^2}{(b+c)\cosh^2(k_M h)} \sin^2(k_M c). \tag{9}$$

When the baffle is a flexible beam-like body and its motion is not large, let's assume that the baffle motion is governed by the Euler-Bernoulli beam equation, i.e.

$$EI \frac{\partial^4 \xi}{\partial y^4} + m_b \frac{\partial^2 \xi}{\partial t^2} = \Delta p(y, t), \tag{10}$$

where $\xi(y,t)$ is the deflection of the baffle and Δp means the pressure difference across the baffle. *EI* and m_b denote the flexural rigidity and mass per unit length of the baffle.

By expanding both the potential and the baffle deflection in their respective modal bases and enforcing the coupling conditions, the hydroelastic problem is reduced to a coupled eigenvalue problem of the form:

$$\left[\mathbf{D} - \omega^2 \mathbf{M}\right]\{\mathbf{A}\} = 0. \tag{11}$$

In this equation, **D** and **M** are system matrices resulting from the application of the boundary and continuity conditions, where **D** contains the stiffness-related and frequency-independent terms, and **M** represents the inertial operator associated with the fluid and the flexible baffle. Vector {**A**} consists of the unknown modal coefficients of the fluid potentials and the flexible baffle deformation.

3 EXPERIMENTAL SCHEME AND TEST CONDITIONS

The experimental setup follows Park et al. [6]. A vertical beam-type baffle was installed at the bottom center as cantilever type, with the same geometry and mounting method as previously used. Flexible baffle material was the Nitrile Butadiene Rubber with a hardness of 80 degrees (NBR 80).

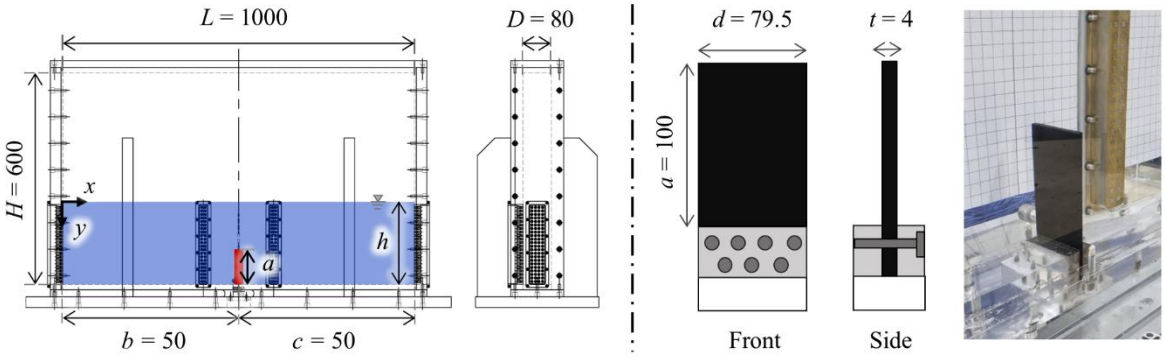

Figure 2: Experimental tank (left) and internal baffle (right), unit: mm

Table 1 summarizes the natural frequencies (ω_n) predicted from the eigenvalue analyses. Differences are clear when the filling height is getting close to baffle height, but the differences are not significant in higher filling levels.

Table 1. Comparison of eigenvalues of natural sloshing mode

h / H (%)	$\omega_n (L / g)^{1/2}$			
	without baffle	with rigid baffle		with flexible baffle
		from Eq. (8)	from Eq. (9)	from Eq. (11)
20	1.064	1.057	0.928	0.853
40	1.415	1.378	1.349	1.361
60	1.597	1.562	1.563	1.629

Regular sway motion was tested with amplitudes (A) of 10-70 mm, while excitation frequencies were varied around the fundamental sloshing frequency of the non-compartmented tank. In this paper, 20% filling condition is the main focus. Baffle deformation and wall pressures were measured using a high-speed camera and clustered pressure sensors, respectively, following the same measurement system as in the previous study.

4 NUMERICAL COMPUTATION: HYDROELASTICITY ANALYSIS

Numerical simulations were conducted to complement the experiments and examine the hydroelastic response of the flexible baffle under sloshing excitation. A strongly coupled two-way fluid-structure interaction framework was employed, in which the fluid solver Star-CCM+ and the structural solver ABAQUS were coupled through a partitioned co-simulation approach. Pressure loads computed in the fluid solver were transferred to the structural solver, and the resulting baffle deformation was fed back to update the fluid domain, ensuring stable synchronized coupling.

The computational model closely followed the experimental configuration. The experimentally measured sway motion was directly imposed in the simulations to maintain consistency between numerical and experimental conditions. The fluid domain was discretized using a finite-volume method, while the baffle was modeled using finite elements with a hyper-elastic Ogden material model to capture large deformations.

5 RESULTS AND OBSERVATION

Figure 3 compares free-surface snapshots at 20% filling condition. For each motion amplitude, the left and right images are referenced to the eigenfrequency of flexible-baffle and the without-baffle tank, respectively. At the lowest excitation amplitude, the free-surface response is most pronounced when the excitation frequency is referenced to the flexible-baffle eigenfrequency derived in previous section, whereas the response is weaker when referenced to the non-compartmented tank eigenfrequency.

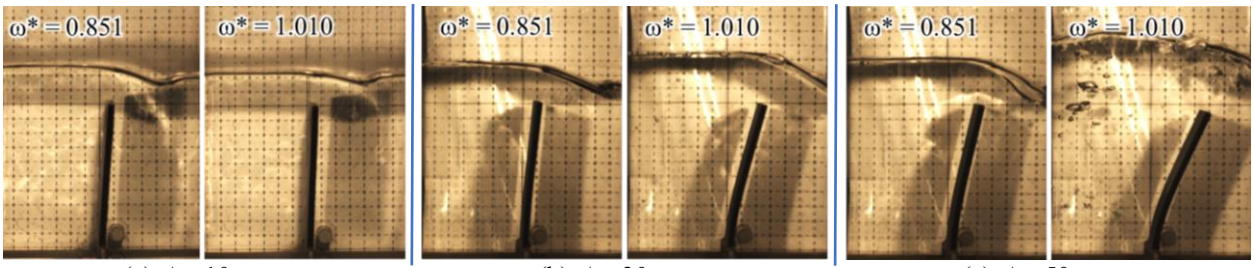

(a) A = 10 mm (b) A = 30 mm (c) A = 50 mm

Figure 3: Free-surface flow and baffle deformation at different motion amplitudes: 20% filling, $\omega^* = \omega(L / g)^{1/2}$

Figure 4 presents the frequency-dependent baffle end-point displacement and dynamic pressure for excitation amplitudes ranging from 10 to 70 mm at the 20% filling condition. The shaded bands indicate the eigenfrequencies predicted for the flexible-baffle (Eq. 11), rigid-baffle (Eq. 9), and without-baffle configurations. The dynamic pressure is quantified using the root-mean-square (RMS) of the differential pressure signals measured between the left and right rear wall panels and normalized by the excitation motion parameters, while the baffle end-point displacement is characterized by the cycle-wise maximum value, allowing a direct comparison of peak response across excitation frequencies.

At A = 10 mm, the normalized baffle displacement does not exhibit a clear peak near the predicted eigenfrequency due to the weak forcing and the normalization effect. In contrast, the pressure asymmetry shows a distinct peak within the flexible-baffle eigenfrequency band, indicating that pressure-based measures are most sensitive indicators of hydroelastic resonance at low amplitudes. This resonance-driven behavior is most pronounced at small amplitudes, while the system response progressively transitions to fully nonlinear characteristics as the excitation amplitude increases.

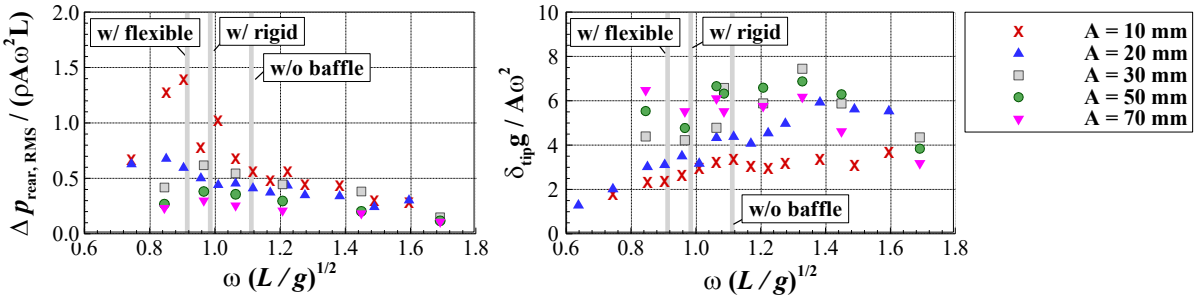

Figure 4: RMS of pressure difference around baffle (left) and end-point displacement (right): 20% filling

Figure 5 compares the normalized baffle tip displacement obtained from the experiments and the coupled fluid-structure interaction (FSI) simulations under a near-eigenfrequency condition with a flexible baffle. The comparison was performed at a motion amplitude of 10 mm. The coupled FSI simulations reproduce the dominant oscillatory response near the flexible-baffle eigenfrequency with reasonable agreement in phase and overall amplitude, confirming the consistency of the eigenvalue-based interpretation. Higher-frequency nonlinear components observed in the experiments are underestimated, indicating the complementary role of the numerical model.

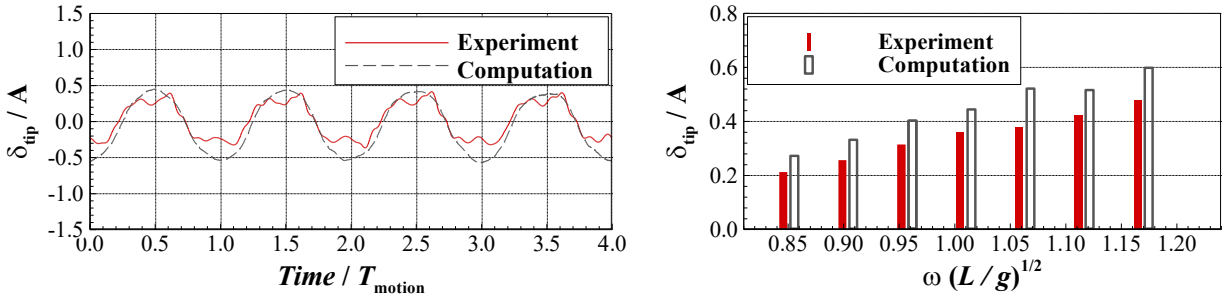

(a) Time signal: A = 10 mm, $\omega\ (L/g)^{1/2}$ = 0.851 (b) Maximum displacement: A = 10 mm

Figure 5: Comparison of displacement at end-point between experiment and numerical simulation: 20% filling

REFERENCES

[1] Evans, D.V., McIver, P., 1987. *Resonant frequencies in a container with a vertical baffle*. Journal of Fluid Mechanics, 175, 295-307.

[2] Jeyakumaran, R., McIver, P., 1994. *Approximations to sloshing frequencies for rectangular tanks with internal structures*. Journal of engineering mathematics, 29(6), 537-556.

[3] Faltinsen, O. M., Timokha, A. N., 2009. *Sloshing*. (Cambridge).

[4] Meng, X., Zhou, D., Wang, J., 2021. *Effect of vertical elastic baffle on liquid sloshing in rectangular rigid container*. International Journal of Structural Stability and Dynamics, 21(12), 2150167.

[5] Ren, Y., Xue, M. A., Lin, P., 2023. *Experimental study of sloshing characteristics in a rectangular tank with elastic baffles*. Journal of Fluids and Structures, 122, 103984.

[6] Park, T., Park, C. J., Lee, J., Kim, Y., 2025. *Experimental observation on violent sloshing flows inside rectangular tank with flexible baffles*. Applied Ocean Research, 154, 104307.